Gene Therapy (2014) **21**, 60–70

www.nature.com/gt

OPEN

ORIGINAL ARTICLE

Therapeutic expression of hairpins targeting apolipoprotein B100 induces phenotypic and transcriptome changes in murine liver

P Maczuga[1,2], J Verheij[3], C van der Loos[3], R van Logtenstein[1], G Hooijer[3], R Martier[1], F Borel[1,4], J Lubelski[1], A Koornneef[1], B Blits[1], S van Deventer[2], H Petry[1] and P Konstantinova[1]

Constitutive expression of short hairpin RNAs (shRNAs) may cause cellular toxicity *in vivo* and using microRNA (miRNA) scaffolds can circumvent this problem. Previously, we have shown that embedding small interfering RNA sequences targeting apolipoprotein B100 (ApoB) in shRNA (shApoB) or miRNA (miApoB) scaffolds resulted in differential processing and long-term efficacy *in vivo*. Here we show that adeno-associated virus (AAV)-shApoB- or AAV-miApoB-mediated ApoB knockdown induced differential liver morphology and transcriptome expression changes. Our analyses indicate that ApoB knockdown with both shApoB and miApoB resulted in alterations of genes involved in lipid metabolism. In addition, in AAV-shApoB-injected animals, genes involved in immune system activation or cell growth and death were affected, which was associated with increased hepatocyte proliferation. Subsequently, in AAV-miApoB-injected animals, changes of genes involved in oxidoreductase activity, oxidative phosphorylation and nucleic bases biosynthetic processes were observed. Our results demonstrate that long-term knockdown of ApoB *in vivo* by shApoB or miApoB induces several transcriptome changes in murine liver. The increased hepatocyte profileration by AAV-shRNA may have severe long-term effects indicating that AAV-mediated RNA interference therapy using artificial miRNA may be a safer approach for familial hypercholesterolemia therapy.

Gene Therapy (2014) **21,** 60–70; doi:10.1038/gt.2013.58; published online 24 October 2013

Keywords: AAV; liver; shRNA; miRNA; ApoB; familial hypercholesterolemia

INTRODUCTION

RNA interference (RNAi) is an evolutionary conserved sequence-specific post-transcriptional gene silencing mechanism in eukaryotes that results in the degradation of mRNA and subsequently in decrease of protein synthesis.[1] Therapeutic RNAi can be induced by delivering synthetic small interfering RNAs (siRNAs) or by intracellular expression of short hairpin RNAs (shRNAs) and artificial microRNAs (miRNAs) that target a disease-causing gene.[2–4] The shRNAs and miRNAs are typically expressed in the cell from pol III or pol II promoters, respectively, and are processed by the RNAi machinery, rendering a mature siRNA that interacts with the cytosolic multiprotein RNA-induced silencing complex. The RNA-induced silencing complex-incorporated siRNA binds to the complementary mRNA sequence and mediates its sequence-specific degradation or translational repression.[5,6]

Because RNAi can interfere with normal functioning of the cells, the safety of RNAi therapeutics is a major issue. Nonspecific effects resulting from RNAi induction appear to have several main causes: oversaturation of the RNAi pathway, aspecific activation of the immune response and off-target effects due to partial complementarity to nontargeted genes.[7–12] These side effects are often associated with severe toxicity, which can be even fatal. High expression levels of therapeutic shRNA can saturate the endogenous RNAi machinery and, in consequence, lead to deregulation of the entire miRNA network.[8] For example, mice injected with adeno-associated virus (AAV)-expressing shRNAs against different targets developed liver failure irrespective of hairpin length, sequence and target.[8] Toxicity could be circumvented by using lower vector doses, but this approach in some cases resulted in loss of RNAi silencing efficacy and therapeutic effect.[13] Alternatively, toxicity resulting from shRNA overexpression can be resolved by embedding the siRNA sequence into an artificial miRNA scaffold and expressing it from weaker pol II promoters.[4,14,15] By using miRNA scaffolds, disruption of the endogenous RNAi pathway is avoided and shRNA-induced cell death can be prevented. However, in some cases, miRNAs were found to be less potent as compared with shRNAs.[13]

A second source of toxicity is immune system activation. Characteristically, the interferon (IFN) response to foreign double-stranded RNAs is either mediated by phosphorylation of the double-stranded RNA-dependent protein kinase R, leading to a global inhibition of protein synthesis,[16] or via Toll-like receptors activation.[17] Recent studies showed that RNAi therapeutics, in particular siRNAs, can be potent inducers of IFN and inflammatory cytokines both *in vivo* and *in vitro*.[10,11] Administration of siRNA for treatment of neovascular age-related macular degeneration has been reported to induce retinal degeneration via nonspecific activation of immune response, which was independent of siRNA or target sequence.[18] Although intracellulary expressed shRNAs are less prone to IFN activation because they can evade activation of Toll-like receptors, several reports indicated immune reactions against vector-delivered shRNA. For example, adenoviral delivery of shRNA targeting fatty acid-binding protein 5 (Fabp5) activated IFN response in liver,[19] and lentiviral vector delivery

[1]Department of Research & Development, uniQure Biopharma B.V., Amsterdam, The Netherlands; [2]Department of Gastroenterology and Hepatology, Leiden University Medical Center, Leiden, The Netherlands; [3]Department of Pathology, Academic Medical Center, Amsterdam, The Netherlands and [4]Department of Gastroenterology and Hepatology, Academic Medical Center, Amsterdam, The Netherlands. Correspondence: Dr P Konstantinova, Department of Research & Development, uniQure Biopharma B.V., Meibergdreef 61, Amsterdam 1105 BA, The Netherlands.
E-mail: p.konstantinova@uniQure.com
Received 19 April 2013; revised 13 August 2013; accepted 16 September 2013; published online 24 October 2013

of shRNA targeting cyclophilin resulted in IFN activation *in vitro*.[20]

Another source of RNAi toxicity is aspecific deregulation of gene expression, when nontargeted transcripts are downregulated based on sequence complementarity to the shRNA or miRNA 'seed' sequence.[12,21] Because of the complexity of shRNA and miRNA processing and RNA-induced silencing complex loading, these unanticipated interactions are difficult to predict and evaluate. Off-targeting can be minimized by adopting a stringent design filter for both sense and antisense strands of the RNAi effector molecules. This approach has been validated for siRNA targeting Huntingtin, where off-targeting effect was significantly minimized by avoiding partial complementarity of siRNA to 3′-untranslated regions of nontargeted genes, whereas a high silencing of Huntingtin was maintained.[22] In addition, significant reduction of off-target effects can be achieved by reducing the dose of siRNA or by chemical modification that impairs siRNA binding to possible off-targets.[23]

Previously, we have identified differences in processing and efficacy of shRNA and artificial miRNA targeting apolipoprotein B100 (ApoB) that resulted in differences in long-term gene silencing *in vivo* when delivered with self-complementary AAV serotype 8.[24] In the present study we investigated the effect of AAV-shApoB and AAV-miApoB expression on liver morphology, cell proliferation, cellular miRNA and transcriptome changes. Using both approaches, a strong decrease of plasma cholesterol was observed *in vivo* without signs of serious side effects. Although biochemical analysis showed no acute toxicity, the AAV-shApoB and AAV-miApoB induced differential changes in liver histology, miRNA and transcriptome profiles. Hepatic steatosis, which is a known side effect of ApoB inhibition, was observed with both molecules. In AAV-shApoB-injected animals, increased proliferation of hepatocytes was observed as compared with AAV-miApoB, and only in AAV-shApoB-injected animals, genes involved in immune response, cell growth and death were found to be affected.

RESULTS

Knockdown efficacy of AAV-delivered shApoB and miApoB in murine liver

We have previously reported that identical AAV-delivered siApoB sequences in shApoB and miApoB scaffolds (Figure 1a) are differently processed that might influence their knockdown efficacy *in vivo*.[24] AAV-miApoB expression was restricted to the liver and resulted in a more sustained reduction of plasma ApoB and cholesterol in mice compared with the ubiquitously expressed AAV-shApoB over 27 weeks of experiment. The reduction of therapeutic efficacy was associated with a loss of virally delivered DNA but no obvious signs of RNAi toxicity were observed. To investigate the possible reasons for loss of DNA, male C57Bl/6 mice were injected with 1×10^{11} genome copies (gc) of AAV encoding shApoB or miApoB targeting the same region of ApoB gene or their respective scrambled controls, shScr and miScr, that are not targeting any sequence in the human or mouse genome. Based on our previous experiments, we speculated that

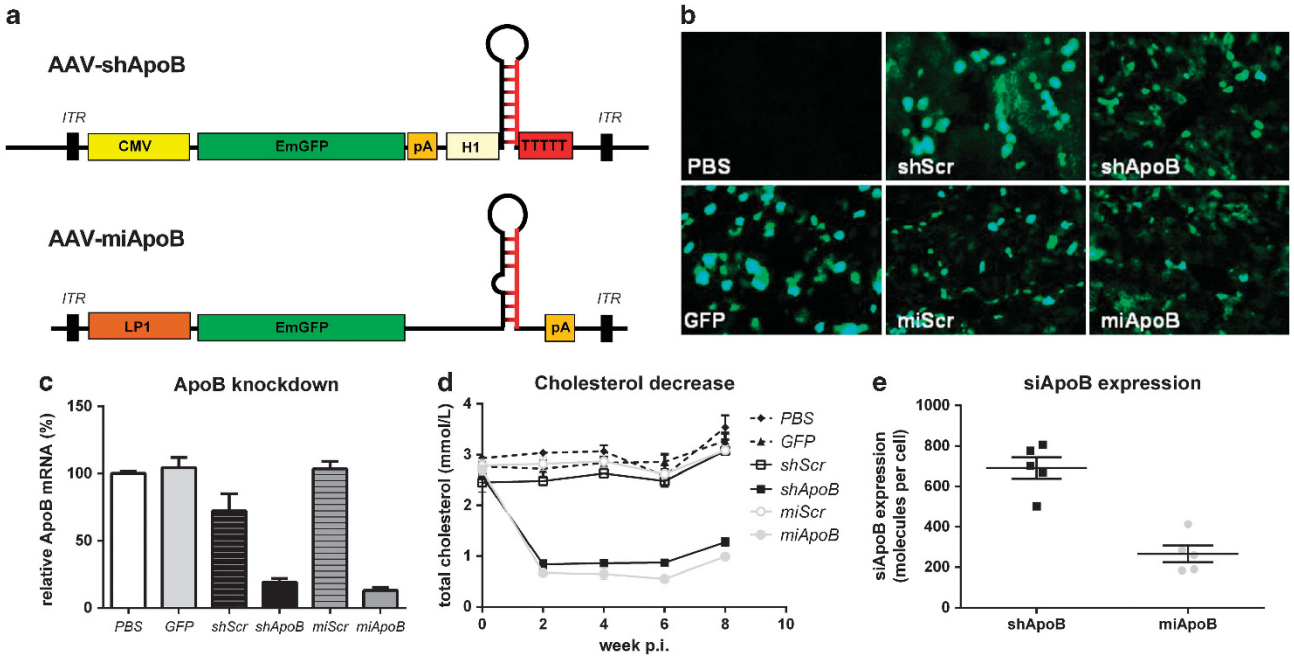

Figure 1. Structure, knockdown efficacy of AAV-shApoB and AAV-miApoB and siApoB expression *in vivo*. Male C57BL/6 mice were intravenously injected with 1×10^{11} gc AAV-shApoB, AAV-miApoB, AAV-shScr, AAV-miScr, AAV-GFP or PBS. Plasma was collected every 2 weeks p.i., animals were killed at 8 weeks p.i. and liver samples were collected for analysis. (**a**) Schematic representation of AAV-shApoB and AAV-miApoB expression cassettes. AAV-miApoB, adeno-associated virus expressing artificial miRNA against apolipoprotein B100; AAV-shApoB, adeno-associated virus expressing short hairpin RNA against apolipoprotein B100; CMV, cytomegalovirus promoter; EmGFP, Emerald green fluorescent protein; H1, H1 promoter; LP1, liver-specific promoter; pA, polyadenylation signal; siApoB, small interfering RNA against apolipoprotein B100; TTTTT, poly U termination signal. (**b**) Representative image of GFP fluorescence in snap-frozen livers, transduced with 10^{11} gc of the indicated viruses or PBS. Photos were taken using the same exposure and magnification settings. (**c**) Relative ApoB mRNA expression in murine liver 8 weeks p.i. Total RNA was isolated from snap-frozen liver tissues and qRT-PCR was performed using ApoB- and actin-specific primers. ApoB mRNA levels were calculated relative to actin mRNA. ApoB mRNA levels in the PBS group was set at 100%. Data are represented as mean values ± s.e. (**d**) Total cholesterol levels in plasma collected from fasted mice over the course of 8 weeks p.i. Cholesterol levels were analyzed on the automated clinical chemistry analyzer Modular Analytics P800. (**e**) siRNA expression in murine liver 8 weeks p.i. Total RNA was isolated from snap-frozen tissues and siApoB-specific small RNA Taqman was performed. siApoB copy number was calculated using a siApoB synthetic RNA oligo standard line. Data are represented as mean values ± s.e.

the cause of virally delivered DNA loss occurs at earlier time point, and therefore mice were killed at 8 weeks post injection (p.i.) and liver samples were collected for histological and molecular analysis. For monitoring of liver transduction efficacy, all viruses coexpressed Emerald green fluorescent protein (GFP). Moreover, virus expressing only Emerald GFP (AAV-GFP) was used as an additional control. According to GFP fluorescence intensity, liver transduction efficacy was ~50% (Figure 1b) and at week 8, ApoB mRNA was reduced by 80% in AAV-shApoB-injected animals and 87% in AAV-miApoB-injected animals as compared with scrambled controls (Figure 1c). This resulted in 60% and 70% inhibition of plasma cholesterol, respectively (Figure 1d). Quantification of siApoB molecules expressed in the liver indicated efficient processing from AAV-shApoB and AAV-miApoB and determined that the observed knockdown effect was sequence specific (Figure 1e).

Expression of shApoB increases hepatocyte proliferation *in vivo*

A histological analysis was performed to evaluate the effect of stable expression of shApoB and miApoB on liver morphology. ApoB suppression results in decreased cholesterol levels because of impairment of very-low-density lipoprotein cholesterol (VLDL-C) and low-density lipoprotein cholesterol (LDL-C) assembly,[25] but can also lead to hepatic triglyceride accumulation.[26–28] Triglycerides are normally incorporated into VLDL, and hepatic accumulation of these lipids can potentially cause steatosis. To investigate the effect of ApoB knockdown on liver morphology, a scoring system was developed and was used to score hematoxylin and eosin liver sections (Supplementary Table 1). Histological analysis revealed no gross changes in liver morphology, and no signs of lobular or portal inflammation or parenchymal necrosis were detected in any group (Figure 2a). However in AAV-shApoB- and AAV-miApoB-injected animals, microvesicular steatosis affecting >67% of the liver tissue was apparent (Table 1 and Figure 2a). In addition, an increase in the hepatocellular mitosis rate was found in AAV-shApoB-injected animals (Table 1). To confirm the scoring results and assess the effect of ApoB knockdown on hepatic lipid accumulation, Oil red O staining was performed on liver sections. Increased accumulation of hepatic lipid content in AAV-shApoB- and AAV-miApoB-injected animals as compared with control groups was detected (Figure 2b). AAV-miApoB injection gave rise to a two- to threefold increase in alanine transaminase (ALT) at week 4 p.i. and aspartate transaminase (AST) at week 6 p.i. (Supplementary Figure 1). No significant increase in liver transaminases for the AAV-shScr-, AAV-shApoB- and AAV-GFP-injected animals was observed. Previously, we have demonstrated that the silencing effect of 1×10^{11} gc AAV-shApoB and AAV-miApoB decreased over time and this was associated with a gradual loss of AAV-delivered DNA.[24] We hypothesized that the loss of (nonintegrated) silencing vector could have resulted from either cell division or cell death. Indeed, histological scoring showed an increase of proliferating hepatocytes in AAV-shApoB-injected animals, but no increase of apoptotic cells was observed in any of the groups (Table 1). To confirm these histological findings, we first examined whether AAV-shApoB or AAV-miApoB administration enhances the proliferative state of the liver cells. Two major types of cells populate the liver lobes: parenchymal cells referred to as hepatocytes and nonparenchymal sinusoidal cells. To distinguish between proliferating hepatocytes and sinusoidal cells, slides were simultaneously stained with antibodies against cytokeratin 18 (CK18), which is a marker for hepatocytes, anti-CD31, a known marker for sinusoidal cells, and the Ki67 antigen, a known marker for cell proliferation (Figure 2c). Surprisingly, the number of proliferating hepatocytes was increased by approximately twofold in AAV-shApoB animals as compared with the AAV-miApoB and control groups (Figure 2d). When livers were stained for cleaved caspase 3, no increased apoptosis was detected in any of the animal groups (Figure 2e).

Table 1. Histological scoring of H&E liver sections

Item	*Average score*					
	shScr	*shApoB*	*miScr*	*miApoB*	*GFP*	*PBS*
Macrovesicular steatosis	0	0	0	0	0	0
Microvesicular steatosis	1	3*	0	3*	0	0
Ballooning	0	0	0	0	0	0
Lobular inflammation	1	1	1	1	1	1
Portal inflammation	1	0	0	1	0	1
Sinusoidal dilatation	0	0	0	0	0	0
Parenchymal necrosis	0	0	0	0	0	0
Hepatocellular mitosis	1	2*	0	0	0	0
Councilman bodies	0	0	1	1	1	1

Abbreviations: ApoB, apolipoprotein B100; GFP, green fluorescent protein; H&E, hematoxylin and eosin; miApoB, miRNA against apolipoprotein B100; PBS, phosphate-buffered saline; shApoB, short hairpin RNA against apolipoprotein B100. Mice were intravenously injected with 1×10^{11} genome copies (gc) of AAV-shApoB or AAV-miApoB, or their respective controls adeno-associated virus (AAV)-shScr, AAV-miScr, AAV-GFP and PBS. Animals were killed at 8 weeks post infection (p.i.) and liver samples were collected for analysis. Paraffin-embedded liver sections were stained with H&E and blind histological scoring was performed. Detailed information about the scoring system used can be found in Supplementary Table 1. *$P < 0.05$ one-way analysis of variance (ANOVA) with Bonferroni post test against PBS.

AAV-mediated expression of shApoB and miApoB does not induce RNAi-related side effects

Overexpression of therapeutic shRNAs and miRNAs can modify the processing of cellular miRNA transcripts as they share the same processing pathway and nuclear export machinery. We investigated whether high expression of shApoB and miApoB competes with the intracellular processing of miRNAs *in vivo*. The endogenous levels of seven highly expressed liver miRNAs were measured *in vivo* at 8 weeks p.i. for all animal groups (Figure 3a). The levels of the liver-specific mir-122 and the broadly expressed miRNAs, let-7a, let-7e, mir-26a and mir-221, were not significantly changed in any of the groups expressing shApoB or miApoB. Expression levels for all miRNAs tested were in the range of 80–200% of the levels measured in phosphate-buffered saline (PBS)-treated animals. Mir-133a and mir-199a expression was two- to threefold upregulated in AAV-miApoB-injected animals as compared with PBS-injected animals. Importantly, mir-133a expression was significantly different in the AAV-miApoB group as compared with the AAV-shApoB group.

Another common source of RNAi toxicity is off-targeting, when nontargeted transcripts are downregulated as a consequence of sequence complementarity to the shRNA or miRNA sequence. In our previous study we have shown that shApoB and miApoB are differentially processed *in vivo* and that a pool of different guide and passenger strands was generated. To investigate possible off-target effects, the Smith–Waterman algorithm was used to predict the most abundant guide and passenger strand variants. A total of 19 genes were predicted as off-targets in the liver for the guide and passenger strand of shApoB and 25 for miApoB. To investigate whether any of the predicted interactions correlates with our experimental data, *in vivo* next-generation sequencing (NGS) data were screened for the predicted off-target gene expression and evaluated for changes (Figure 3b). From the 19 predicted off-target genes, 11 were expressed in AAV-shApoB animals and 10 in AAV-miApoB-injected animals. Surprisingly, the expression of none of the predicted off-targets for both shApoB and miApoB was significantly changed *in vivo* (Figure 3b).

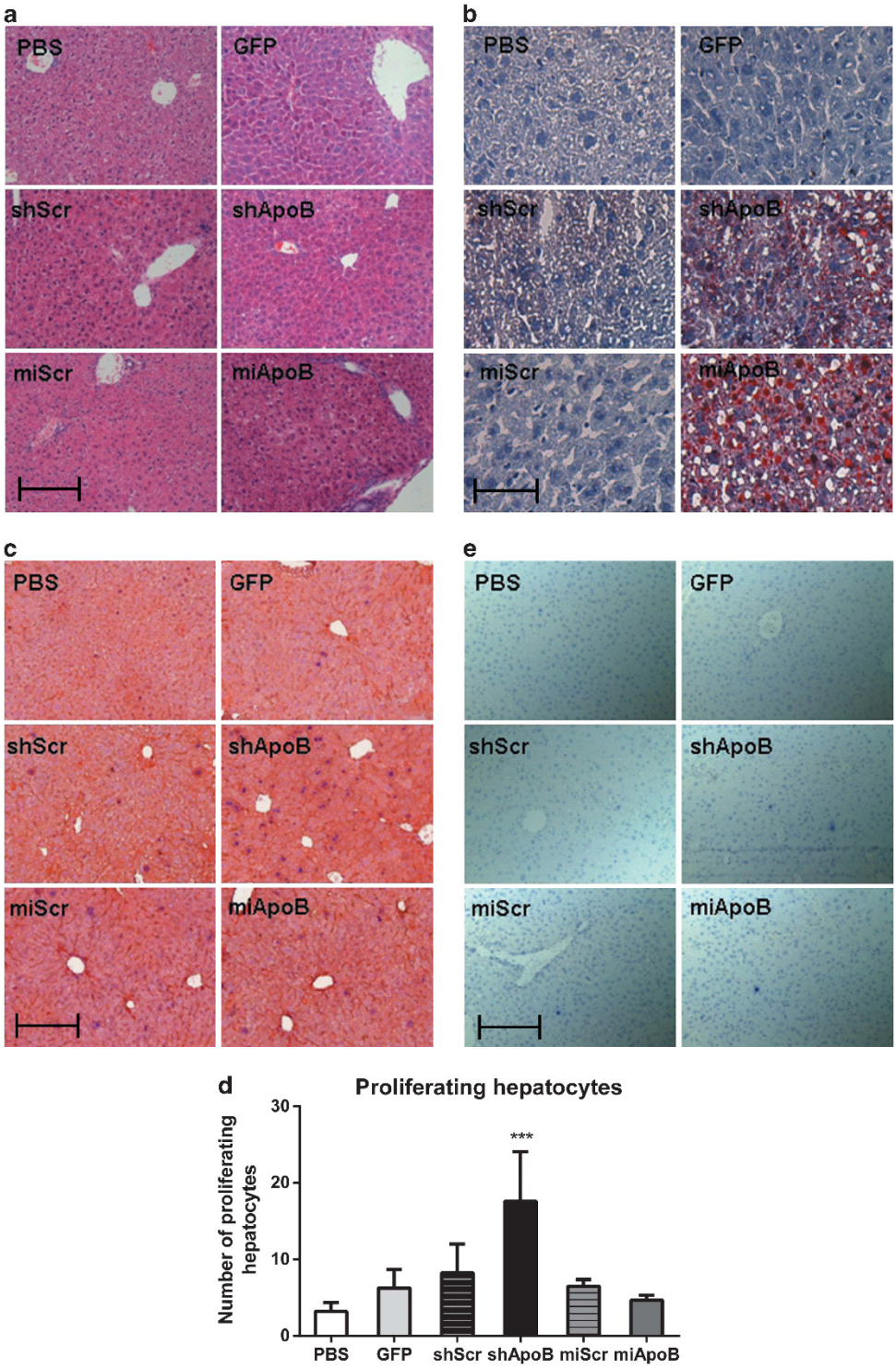

Figure 2. Effect of AAV-delivered shApoB and miApoB on liver morphology, proliferation and hepatic fat accumulation. Mice were intravenously injected with 1×10^{11} gc AAV-shApoB or AAV-miApoB, or their respective controls AAV-shScr, AAV-miScr, AAV-GFP and PBS. Animals were killed at 8 weeks p.i. and liver samples were collected for analysis. (**a**) Representative image of hematoxylin and eosin (H&E) liver morphology staining. Paraffin-embedded liver sections were stained with eosin for cytoplasm visualization, and nuclei were counterstained with hematoxylin solution. (**b**) Representative image of hepatic lipid accumulation. Frozen liver sections were stained with Oil Red O for lipids, and nuclei were counterstained with hematoxylin solution. (**c**) Representative image of liver proliferation. Paraffin-embedded liver sections were simultaneously stained in red for hepatocytes (rabbit anti-mouse CK18), in brown for sinusoidal cells (rabbit anti-mouse CD31) and in blue for antigen Ki67 (rabbit ant-mouse Ki67). A nuclei counterstaining with hematoxylin was performed. (**d**) Quantification of proliferating hepatocytes staining as described in (**c**). Spectral decomposition was done using InForm software v1.4 (PerkinElmer/Caliper Life Science) and the amount of proliferating hepatocytes (CK18 +, Ki67 +) was calculated for each animal in five different visual fields. Data are represented as mean values of five animals ± s.e. ***$P < 0.001$ one-way analysis of variance (ANOVA) with Bonferroni post test against PBS. (**e**) Representative image of liver apoptosis. Paraffin-embedded liver sections were stained in blue for cleaved-caspase 3 (rabbit anti-mouse). Nuclei counterstaining with hematoxylin was performed. Bar, 5 μm.

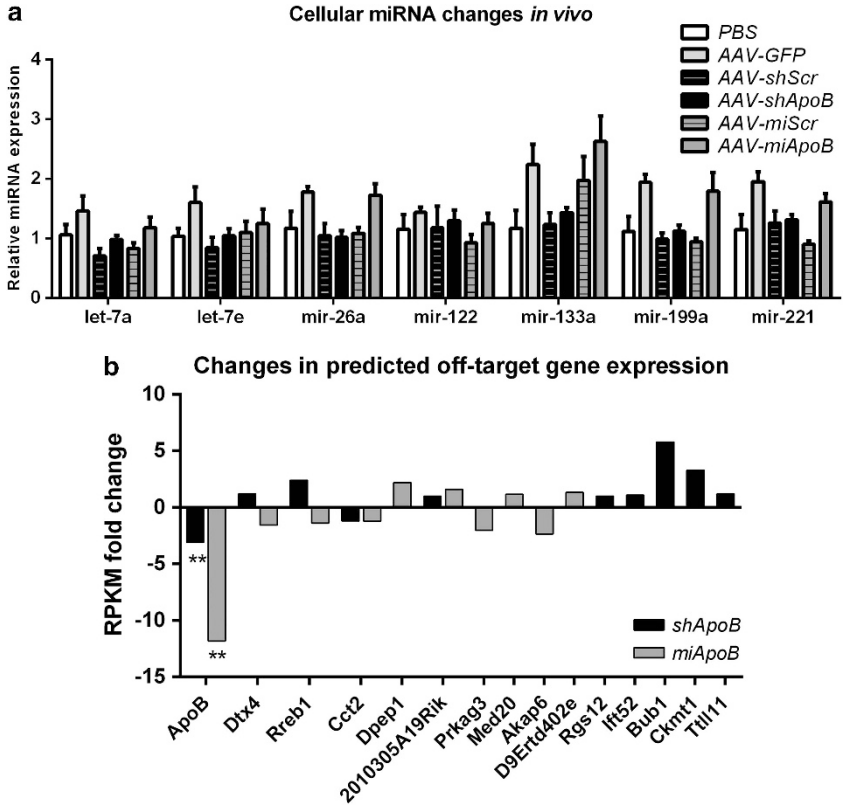

Figure 3. Effect of shApoB and miApoB expression on cellular miRNA and off-target gene expressions. (**a**) Relative expression of let-7a, let-7e, mir-26a, mir-122, mir-133a, mir-199b and mir-221 *in vivo* was measured by miRNA Taqman. Mice were intravenously injected with 1×10^{11} gc AAV-shApoB or AAV-miApoB, or their respective controls AAV-shScr, AAV-miScr, AAV-GFP and PBS. Total RNA was isolated from snap-frozen livers. miRNA expression levels were calculated relative to actin mRNA and the PBS-treated group was set at 100%. Data are represented as mean + s.e., treatment groups are $n = 5$. (**b**) Changes in predicted shApoB and miApoB off-target gene expression. Smith–Waterman algorithm was used to predict shApoB and miApoB off-target genes for the most abundant expressed variants of passenger and guide strands in mouse reference genome (15 May 2012 NCBI build 38.1). Predicted targets were manually screened for genes expressed in the liver that were detected in NGS transcriptome analysis. Gray and black bars represent fold change in AAV-shApoB and AAV-miApoB relative to AAV-shScr or AAV-miScr controls respectively. Kal's test (*Z*-test) with Bonferroni correction was used to compare the RPKM value in the shApoB versus shScr or miApoB versus miScr. $^{**}P < 0.01$.

NGS of liver transcriptome reveals differential gene expression in AAV-shApoB- and miApoB-injected animals

The differential siRNA processing from shRNA or miRNA scaffolds may have different consequences for induction of aspecific off-target effects. Therefore, we investigated the effect of AAV-shApoB, AAV-shScr, AAV-miApoB, AAV-miScr or PBS on the liver transcriptome by performing NGS analysis. The expression abundance for each gene, represented in reads per kilobase of exon model per million mapped reads (RPKM), was calculated and Kal's test (*Z*-test) with Bonferroni correction was used to compare the RPKM values. We further focused on gene changes that are specific results of shApoB and miApoB expression, and therefore we compared their profiles with the negative controls AAV-shScr and AAV-miScr. All AAV viruses coexpressed GFP, and therefore the AAV-GFP sample was excluded from the NGS analysis. In the AAV-shApoB sample, 106 genes were found to be significantly changed (68 were upregulated and 38 were downregulated; $P < 0.05$) as compared with AAV-shScr (Figure 4a). A total of 266 genes were significantly changed ($P < 0.05$) in AAV-miApoB-treated mice as compared with AAV-miScr. Among them, 154 genes were upregulated and 112 genes were found to be downregulated (Figure 4a). To confirm the changes observed in the NGS analysis, ApoB knockdown measured with NGS, quantitative real-time reverse transcription-PCR (qRT-PCR) and western blot was compared (Figure 4b and data not shown). For both AAV-shApoB and AAV-miApoB animal groups, ApoB knockdown detected with NGS correlated with qRT-PCR and western blot data, indicating that NGS analysis is a reliable method for comparing gene expression between the different animal groups.

Knockdown of ApoB can influence the expression of genes functionally related to ApoB. Therefore, we performed a detailed analysis on the expression changes of 44 ApoB predicted partner genes in AAV-shApoB and AAV-miApoB animals versus their respective Scr controls (Figure 4c). The expression of most of the genes was only marginally affected, indicating that ApoB knockdown had no severe aspecific effect on the expression changes of genes involved in cholesterol metabolism. Interestingly, the expression changes of Apobec2, Bgn and Lpl followed the same trend in both animal groups. The biggest fold changes were observed for ApoA4 where gene expression increased 6.18-fold in the AAV-shApoB animal and decreased 8.86-fold in the AAV-miApoB animal. The NGS analysis was performed on one animal per group and one should interpret the data with care because it may show some individual variation. To verify our observations, we performed qRT-PCR analysis of the expression of 18 selected ApoB partner genes (7 high, 7 medium and 4 low expressed) on more animals from the different experimental groups (Figure 4d and Supplementary Figure 2). Interestingly, expression changes of all genes followed the same or similar trend in the qRT-PCR and NGS analysis with the exception of the shApoB group where no

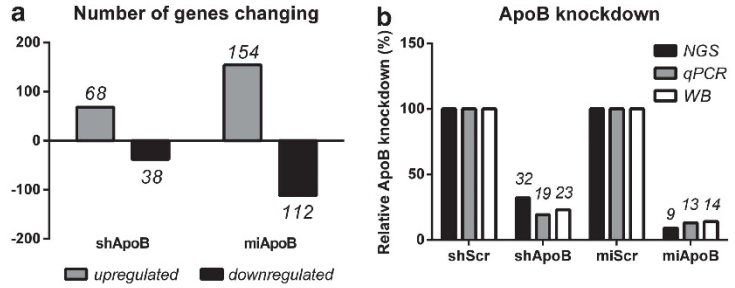

c

ApoB predicted partners' expression changes

	A1cf	Abca1	Abcg5	Acat1	Apoa1	Apoa2	Apoa4	Apoa5	Apobec1	Apobec2	Apobec3
shApoB	1,21	1,33	1,05	1,07	-1,13	-1,50	6,18	-1,20	1,77	-2,25	1,83
miApoB	-3,16	-1,95	-2,53	1,73	1,16	2,03	-8,86	-1,01	1,02	-2,50	1,32

	Apoc2	Apoc3	Apoe	Apom	Bgn	Cd320	Cda	Ces3b	Cog2	Cyp7a1	Eif4g2
shApoB	1,56	-1,62	-1,23	-1,05	1,67	1,38	1,19	-1,68	1,54	1,76	1,26
miApoB	-1,08	1,26	1,50	1,15	1,77	2,43	1,94	1,25	1,09	1,27	-1,26

	Fgr	Hspg2	Lcat	Ldlr	Ldlrap1	Lipc	Lpl	Lsr	Mtp	Mvp	Nr1h4
shApoB	2,89	1,31	-1,35	1,23	1,66	1,08	1,88	1,02	-1,06	1,48	-1,01
miApoB	1,31	-1,24	-1,31	-1,75	1,06	1,05	6,18	-1,24	1,36	1,10	1,13

	P4hb	Pcsk9	Plg	Plk1	Pltp	Ppara	Scarb1	Sdc1	Srebf2	Txn1	Txnip
shApoB	-1,10	1,02	-1,10	4,16	1,14	1,06	1,42	1,62	1,35	-1,11	1,29
miApoB	-1,46	-2,70	-1,30	-2,09	1,03	-1,32	-1,80	1,45	-1,59	1,63	-1,09

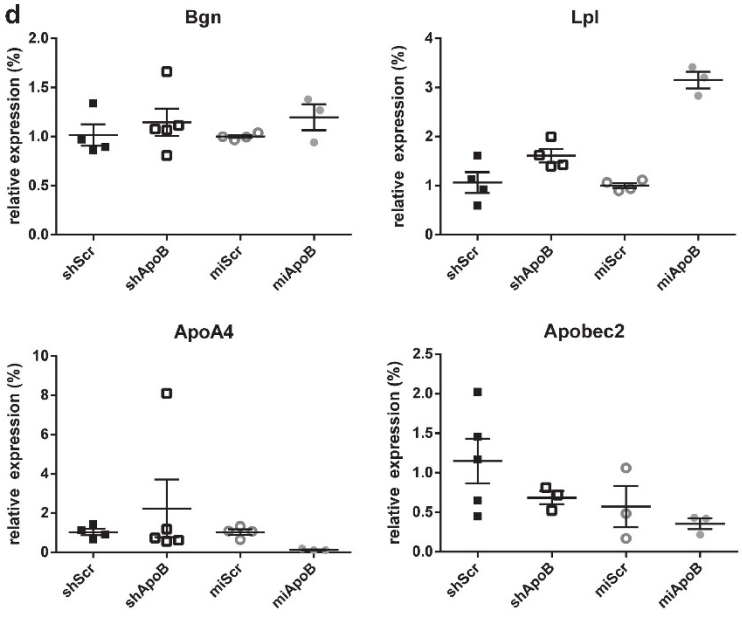

Figure 4. NGS transcriptome analysis on gene expression profiles between AAV-shApoB- and AAV-miApoB-injected animals. To analyze liver transcriptome, total RNA was isolated from a representative animal 8 weeks p.i. and NGS analysis was performed. The expression abundance for all genes was quantified using the RPKM measure. Expression data were compared using Kal's *Z*-test with Bonferroni correction. Genes that showed a significantly altered expression ($P<0.05$) were used in further analysis. (**a**) Genes significantly upregulated or downregulated in AAV-shApoB- and AAV-miApoB-injected animals. Gray and black bars represent number of genes upregulated and downregulated, respectively, compared with AAV-shScr or AAV-miScr controls ($P<0.05$). (**b**) Comparison of ApoB knockdown *in vivo* by NGS, qRT-PCR and protein western blot. In all assays, ApoB expression levels were calculated relative to AAV-shScr or AAV-miScr, which served as negative controls and were set at 100%. (**c**) Prediction of ApoB functional interactions was performed with STRING software.[49] Upregulated genes (fold change >1.5) were marked in green and downregulated (fold change <-1.5) were marked in red. (**d**) qRT-PCR analysis of Bgn, Lpl, ApoA2 and Apobec2 expression in murine liver 8 weeks p.i. Total RNA was isolated from snap-frozen liver tissues and qRT-PCR was performed with Bgn-, Lpl-, ApoA2-, Apobec2- and actin-specific primers. mRNA levels were calculated relative to actin mRNA. Expression levels in the shScr and miScr were set as 100% for shApoB and miApoB groups, respectively. Data are represented as individual measurements with mean values ± s.e. plotted.

upregulation of ApoA4 and Plk1 was observed. Careful examination of the data indicated that the AAV-shApoB-injected animal that was analyzed with NGS had upregulated ApoA4. Same result was also obtained in qRT-PCR analysis, indicating that this animal was an outlier and confirming the robustness of our NGS analysis (Figure 4d and Supplementary Figure 2). Notably, there were no significant

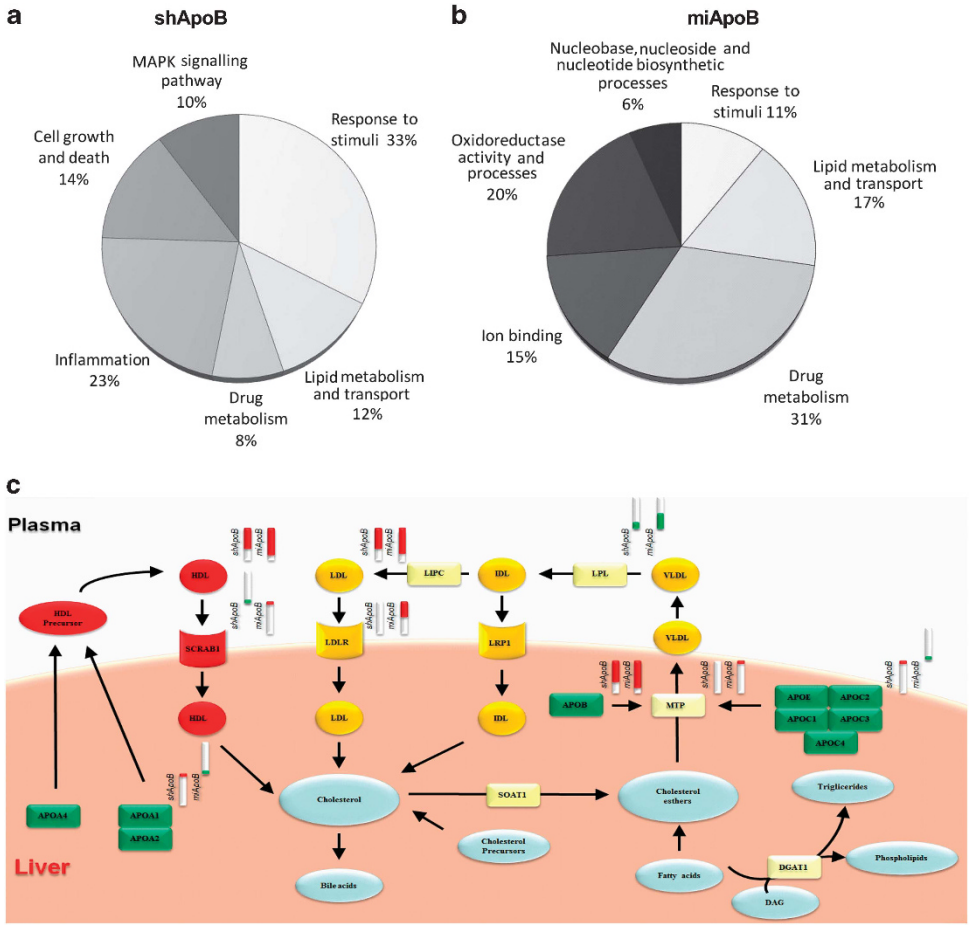

Figure 5. Functional categorization of gene expression changes in AAV-shApoB- and AAV-miApoB-injected animals. (**a**, **b**) Percentage and functional categorization of genes that are significantly changed in expression in AAV-shApoB and AAV-miApoB animal groups. Up- and downregulated genes in AAV-shApoB and AAV-miApoB groups ($P<0.05$) were annotated to Gene Ontology (GOTERM_BP_FAT and GOTERM_MF_FAT) and KEGG (KEGG_PATHWAY) using the DAVID v6.7 (National Institute of Allergy and Infectious Diseases (NIAID), NIH). Significant annotations ($P<0.05$) were grouped in eight categories and the percentage of genes in each category was calculated with reference to all genes annotated in the DAVID analysis. (**c**) Outline of cholesterol pathway changes in AAV-miApoB- and AAV-shApoB-injected animals. There are several types of lipoproteins within blood: chylomicrons, very-low-density lipoprotein (VLDL), intermediate-density lipoprotein (IDL), low-density lipoprotein (LDL) and high-density lipoprotein (HDL). ApoB100 protein is synthesized in the liver and it forms the structural protein in VLDL and LDL particles. HDL is secreted by the gut and liver and receives additional components during the metabolism of triglyceride-rich lipoproteins. Therefore, inhibition of ApoB affects VLDL-C, LDL-C and HDL-C levels. Genes significantly altered in the AAV-shApoB and AAV-miApoB groups were used ($P<0.05$) for toxicology prediction using Metacore software (Thomson Reuters, New York, NY, USA) and the top-scored map was generated. Experimental data from AAV-shApoB and AAV-miApoB groups are linked to and visualized on the image as thermometer-like figures placed in the top right of respective gene or group of genes. Upward red-colored thermometers indicate upregulated components and downward blue thermometers indicate downregulated components of the pathway.

gene expression changes between AAV-GFP- and PBS-injected animals, indicating that the observed effects are not AAV specific.

Functional categorization of the NGS data

To generate a full functional profile for all genes altered by the *in vivo* expression of shScr, shApoB, miScr and miApoB, a web-based tool DAVID (Database for Annotation, Visualization and Integrated Discovery) was used for the ontological analysis of large lists of genes (see Materials and methods). Analysis of the 106 genes that were significantly changed in the AAV-shApoB group indicated that the most significant functional alterations were related to genes involved in lipid metabolism and transport and response to stimuli (Figure 5a). In addition, expression of genes involved in drug metabolism, inflammation, cell growth and death and the mitogen-activated protein kinase signaling pathway were altered. In the AAV-miApoB animal group, the 266 significantly altered genes corresponded mainly to genes involved in drug metabolism, oxidoreductase activity and processes (Figure 5b). Other relevant pathways include lipid metabolism and transport, ion binding, response to stimuli and nucleobase, nucleoside and nucleotide biosynthetic process. A complete list of genes functionally annotated with DAVID for miApoB and shApoB samples can be found in Supplementary Tables 2 and 3, respectively. Both shApoB and miApoB resulted in potent inhibition of ApoB that exerted expression changes of other lipid metabolism genes (Figure 5c). In both AAV-shApoB and AAV-miApoB groups, ApoA4, Apobec2 and Lpl genes were changing in expression more than twofold. The expression of most of the other genes that encode structural components of very low-density lipoprotein cholesterol (ApoE, ApoC1, ApoC2, ApoC3, ApoC4), high-density lipoprotein cholesterol (ApoA1) and genes involved in cholesterol homeostasis was marginally changed (less than twofold).

Although both shApoB and miApoB were found to affect response to stimuli and drug metabolism, only the serine protease

inhibitors Serpina1b, Serpina1c, Serpina1d and Serpina3k were simultaneously affected in both groups. Serpins compose a large family of the functional diverse proteins that are involved in numerous intracellular and extracellular functions: blood clotting, inflammation, storage, hormone carriage and tumor suppression.[29–31] Only AAV-shApoB injection was found to upregulate genes involved in inflammatory response such as Serpina 8N that is induced during inflammation and serum amyloid A1 (Saa1), a major acute phase reactant. Importantly, the biggest changes in AAV-shApoB-injected animal were observed for Fos (124-fold), Jun (19-fold), Nr4a1 (60-fold), Egr1 (13-fold), Dusp1 (5-fold) and Dusp6 (5-fold). Fos, Jun, Nr4a1m and Egr1 are transcription factors involved in a number of cellular processes including differentiation, proliferation and apoptosis,[32] and Nr4a1 plays a key role in mediating inflammatory responses in macrophages.[33] Dusp1 and Dusp6 negatively regulate the members of the mitogen-activated protein kinase family pathways c-Jun N-terminal kinase and p38, which results in cell apoptosis.[34]

The biggest changes between the two groups were among cytochrome *P*450 family members that are involved in drug and steroid metabolism. Cyp4a14, Cyp4a10 and Cyp2c29 were upregulated 10-, 5- and 3-fold, respectively, in the AAV-miApoB sample, whereas Cyp2a4, Cyp2c67, Cyp1a2, Cyp2c54 and Cyp2f2 were downregulated 9-, 6-, 3-, 3- and 3-fold, respectively, in the AAV-shApoB sample. Other genes that were upregulated in AAV-miApoB-injected animal are involved in oxidoreductase activity, oxidative phosphorylation and nucleic bases biosynthetic processes. Most of these are structural components of mitochondrial oxidative phosphorylation system: NADH-coenzyme Q oxidoreductase (complex I), cytochrome bc1 complex (complex III), cytochrome *c* oxidase (complex IV) and ATP synthase (complex V). Finally, genes involved in lipid metabolism and transport that encode alcohol dehydrogenase (Adh1), acetyl-Coenzyme A acyltransferase (Acaa1b, Acaa1a, Acaa2) and aldehyde dehydrogenase 3 family (Aldh3a2) were upregulated in the AAV-miApoB sample.

DISCUSSION

The major challenge for the RNAi-based therapies is the delivery of siRNAs to the target tissue or organ for stable and long-term inhibition of a disease-related gene. Recent reports on the RNAi toxicity have initiated a discussion about the safety of such an approach. Although in the past few years much progress has been made in understanding the causes of toxicity and approaches to preclude adverse effects have been suggested, detailed studies on the differences between shRNA- or artificial miRNA-encoding constructs and the consequences for *in vivo* applications have not been reported. By using AAV delivery, we have compared the safety profiles of identical predicted siApoB sequences expressed as shApoB and miApoB in long-term *in vivo* studies. Detailed histological and transcriptome analyses revealed several differences between AAV-shApoB- and AAV-miApoB-injected animals, indicating that careful monitoring is necessary before proceeding to clinical trials.

In vivo toxicity of shRNA was often linked to upregulation of liver enzymes ALT and AST in mice[7,8] and in non-human primates.[35] In our experiment, transient activation of liver transaminases was observed in AAV-miScr and AAV-miApoB animals during the course of the experiment, indicating mild dose-dependent toxicity. We have previously reported that such toxicity can be abolished by lowering the administered viral dose.[24] In contrast to our results, Ahn *et al*.[9] described increased ALT levels 3 weeks p.i. after injection of adenovirus encoding shRNA against transcription factor Srebp1 and lipid transporter Fatbp5. Interestingly in their study, the scrambled control hairpin also resulted in increased ALT levels, indicating that toxicity was associated with shRNA expression and was not due to the used adenoviral vector. In another study, 73% of the tested shRNAs resulted in liver injury, whereas expression of others was well tolerated.[8] Although a transient ALT and AST increase was detected in AAV-miScr- and AAV-miApoB-injected animals, no acute inflammation and no gross changes of liver morphology in these groups were detected.

Similar to previous studies, ApoB knockdown by AAV-shApoB and AAV-miApoB resulted in hepatic fat accumulation.[36,37] Surprisingly, steatosis was not observed in murine studies with an ApoB antisense oligonucleotide.[38] However, clinical trials with the human ApoB antisense oligonucleotide did reveal a trend toward an increase in intrahepatic triglyceride content.[28] Steatosis may be associated with inflammation and may progress to cirrhosis, and therefore careful consideration and investigation of this consequence of lowering ApoB is necessary. Tep *et al*.[39] reported that simultaneous silencing of Mtp and Dgat2 rescues ApoB siRNA-induced hepatic steatosis. However Dgat2 silencing resulted in a significant increase of plasma ketones, making this approach not attractive for clinical applications as elevated serum ketones can cause medical emergency. In contrast, double knockdown of ApoB and Dgat2 or Fabp5 did not result in reduction of lipid accumulation.

We observed that injections of AAV-shApoB, but not AAV-miApoB, caused increased hepatocyte proliferation. The reason for the observed proliferation would be hepatocyte damage because of RNAi-induced toxicity. Increased apoptotic and proliferative activity has been observed in murine liver expressing AAV-delivered shRNA targeting human α1-antitripsin[8] and adenoviral-expressed shRNA targeting Srebp1 and Fabp5.[9] In our experiments we observed increased proliferation that was not associated with apoptosis, implying that apoptosis may have occurred earlier than 8 weeks p.i. with AAV-shApoB. Another reason for the increased proliferation could be the hepatic steatosis. Indeed, it has been reported that an increase in liver triglycerides may lead to increased oxidative stress in hepatocytes and lipid-activated apoptosis.[40] However, the fact that miApoB does not affect liver proliferation excludes this possibility. Based on our data and previous reports, we can conclude that increased liver proliferation due to shApoB expression is hairpin structure and dose dependent. It has to be noted that shApoB was expressed from H1 promoter that provide higher expression levels and there are important differences in shApoB and miApoB processing. Importantly, AAV-miApoB- and AAV-miScr-injected animals did not reveal signs of increased liver proliferation, which could have serious consequences for long-term correction, as AAV DNA forms episomal nuclear concatamers in the host cell nucleus, which are lost following cell division.[41] Those results also explain our previous observations where the silencing effect in AAV-shApoB-injected animals was less sustained than in AAV-miApoB-injected animals.[24] In addition, in our previous study we have reported that there are differences in siRNA processing from shApoB and miApoB.

In the current study, a detailed NGS transcriptome analysis revealed substantial gene changes among genes involved in lipid metabolism and transport. Interestingly, Bgn, a proteoglycan that can bind ApoB-containing lipoproteins and is involved in atherosclerosis,[42] and Lpl, which is one of the key enzymes for lipoprotein catabolism that hydrolyzes triglycerides and VLDL-C,[43] were upregulated for both AAV-shApoB and AAV-miApoB. In addition to lipolysis, Lpl mediates the uptake and degradation of lipoproteins by cells. Our hypothesis is that the upregulation of these two genes might be a compensatory reaction to the strong ApoB decrease in murine liver, but the biological significance of those changes needs to be determined. Apobec2, which is an ApoB mRNA editing enzyme, was downregulated in both treatment groups, probably as a result of the low concentrations of ApoB in the liver of shApoB and miApoB animals.

Although Apobec2 functions in liver are not fully investigated, its upregulation has been associated with tumorigenesis and development of hepatocellular carcinoma through hepatic inflammation.[44] Nevertheless, Apobec2-deficient mice did not reveal any abnormalities on health and survival.[45] Some mildly changing genes followed different trends in the AAV-shApoB and AAV-miApoB groups but the biological significance of such minor differences is doubtful and needs to be verified further. Based on our NGS and qRT-PCR analysis, we can claim that ApoB knockdown affects genes that are directly linked to the cholesterol homeostasis.

Recently, significant changes in many lipid metabolism genes following ApoB silencing with siRNA have been reported using Taqman analysis.[39] Out of the 96 genes that were investigated, 53 were downregulated more than 1.5-fold, whereas only 7 were upregulated. However, when compared with our NGS data, only a few genes had a similar change in expression profile (Supplementary Table 4). This may suggest that siRNA, shRNA and miRNA induce different gene expression profile despite the same phenotypic effect. However, it has to be noted that the siApoB used had a different sequence and the experiment was performed in Ldlr/Cetp $+/-$ hemizygous mice, which exhibit different lipid profile. In addition, the analysis was performed 2 weeks p.i. with siApoB, and at this time point gene expression changes may have been more pronounced. To our knowledge, comparison of liver gene expression analyses after siRNA, shRNA and miRNA administration has not been performed.

Besides lipid metabolism and transport, other functions were also altered in murine liver by expression of AAV-shApoB or AAV-miApoB. Response to stimuli and drug metabolism were found to be affected in both shApoB and miApoB groups, but the genes involved showed minimal overlap. shApoB was found to affect genes involved in cell growth and death, inflammation and mitogen-activated protein kinase pathway, which correlated with our findings on increased liver proliferation. In contrast, in the miApoB group, the biggest changes were observed for genes involved in ion binding, nucleobase biosynthetic process and oxidative activity and processes. Previously, Ahn *et al.*[9] described significant transcriptomic changes in mice after adenoviral delivery of shRNA, where a total number of 181 genes were found to be upregulated whereas only 32 genes were found to be downregulated as a consequence of shRNA expression. Data generated from their study suggested that shRNA expression also upregulated genes involved in the RNAi pathway and proliferation. In contrast, we did not show significant upregulation of those genes, which might be because of the fact that we performed our analysis 8 weeks p.i. and because we used AAV as a delivery vector. Importantly, we detected upregulation of inflammatory related genes exclusively in the AAV-shApoB group, although no signs of inflammation in the liver could be found, and in our previous experiments we did not measure IFN response activation.[46] Immune activation might indeed have caused hepatocyte damage in the AAV-shApoB sample, resulting in increased proliferation and eventually loss of the knockdown effect.

In summary, our findings demonstrate that long-term knockdown of ApoB *in vivo* by shApoB or miApoB induces several transcriptome changes in murine liver. However, most of the genes directly linked to ApoB expression changed relatively mildly, indicating that AAV-mediated RNAi therapy can be a safe approach for familial hypercholesterolemia therapy. Previously, we have shown that by lowering AAV viral dose, stable reduction of ApoB and plasma cholesterol can be achieved. Therefore, liver morphology, miRNA and transcriptome profiles need to be investigated when lower AAV doses are used. However, we can claim that a safe gene therapy approach can be achieved by using a minimal AAV dose, in combination with a tissue-specific expression of the RNAi effector molecules.

MATERIALS AND METHODS

DNA constructs, AAV production and purification

The design and cloning of the shApoB, shScr, miScr, miApoB and GFP expression vectors, scAAV8 vector production and purification have been described previously.[24,46] shApoB and miApoB are targeting the same region of ApoB gene (ApoB, NM_000384; 13684-13702).

In vivo experiments

All animal experiments were conducted according to the guidelines of the local animal welfare committee. Male C57BL/6 mice, 6–8weeks old, received an intravenous AAV injection of 1×10^{11} gc per animal ($\sim 4 \times 10^{12}$ gc per kg) via the tail vein. Treatment groups were $n = 5$, mice were housed 6 per cage and feeding was performed *ad libitum* with regular chow. Heparinized blood samples were taken every 2 weeks p.i. from fasted mice. Mice were killed at 8 weeks p.i. and liver and plasma were collected for analysis. Plasma levels of ALT, AST and total cholesterol were analyzed on the automated clinical chemistry analyzer Modular Analytics P800 (Roche Diagnostics, Basel, Switzerland) at the Academic Medical Center (Amsterdam, The Netherlands). Statistical analysis was performed by analysis of variance testing with Bonferroni posttest and $P < 0.05$ was considered significant.

GFP expression was analyzed in snap-frozen liver sections. Livers were cryosectioned at 5 μm and GFP signal was visualized using standard fluorescence microscopy on a Leica fluorescent microscope (Leica Microsystems GmbH, Wetzlar, Germany). For analysis of liver fat accumulation, snap-frozen liver sections were cryosectioned at 5 μm, fixed in 10% formalin and stained for 25 min in filtered 0.3% Oil red O (Sigma, St Louis, MO, USA) solution in 60% isopropanol. Nuclei were counterstained for 5 min in hematoxylin solution (Sigma). Liver histology was assessed by hematoxylin and eosin staining of frozen liver sections.

Immunohistochemistry

Mouse liver samples were fixed with 4% neutral buffered formalin for 48 h and then routinely processed to paraffin blocks. Then, 5 μm sections were cut, mounted on coated slides and dried overnight at 37 °C. Slides were dewaxed in xylene and hydrated with the use of graded alcohols to tap water. Endogenous peroxidases were blocked by incubation in methanol supplemented with 0.3% peroxide. Heat-induced endogenous antigen retrieval was performed in the PreTreatment Module (PTModule; Thermo Fisher Scientific/Labvision, Fremont, CA, USA) for 20 min at 98 °C and a cool-down to 75 °C in Tris-HCl + EDTA, pH 9.0. After washing sections with running tap water, a non-serum protein block Ultra V Block (Thermo Fisher Scientific/Labvision) was applied for 10 min at room temperature. A sequential triple staining procedure[47] started with CD31 (LifeSpan Biosciences Inc., Seattle, WA, USA) visualized by horseradish peroxidase-conjugated anti-rabbit IgG polymer and BrightDAB (both from Immunologic, Duiven, The Netherlands). The DAB reaction product effectively shelters the first set of antibodies and thus prohibits unwanted crossreactions with later incubation steps. Staining was continued with anti-Ki67, clone SP6 (Thermo Fisher Scientific/Labvision) visualized by BrightVision alkaline phosphatase-conjugated anti-rabbit IgG polymer (Immunologic) and Vector Blue (Vector Laboratories, Burlingame, CA, USA). Next, a second heat-induced endogenous antigen retrieval step (10 min, 98 °C) using citrate buffer, pH 6.0, was applied to remove all antibodies used but leaving the chromogens unchanged. Finally, CK18 (Abcam, Cambridge, UK) was visualized by BrightVision alkaline phosphatase conjugated anti-mouse IgG polymer (Immunologic) and Vector Red (Vector Labs). Slides were weakly counterstained with hematoxylin diluted 1:5 in distilled water for 3 min, washed with tap water, completely dried at a hot plate and non-aqueous coverslipped with VectaMount (Vector Labs). Primary and secondary antibodies used in this study are listed in Supplementary Table 5. Antibodies and conjugates were diluted in antibody diluent (Immunologic) and Tris-buffered saline was used as washing buffer for all further steps (three changes, 3 min each). Horseradish peroxidase activity in brown was developed with Bright DAB (Immunologic) according to the manufacturer's instructions. Alkaline phosphatase activity in blue and in red was developed with the Vector Blue and Vector Red kits (Vector Laboratories) with the use of a Tris-HCl buffer (100 mM, pH 8.2) according to the manufacturer's instructions.

Spectral imaging and proliferation quantification

Specimens were observed with a Leica BM5000 microscope equipped with plan apochromatic objectives (Leica Microsystems). From all

immunohistochemistry triple-stained slides, multispectral data sets of five random fields with Ki67-positive nuclei at $\times 200$ were acquired using a Nuance imaging system (PerkinElmer/Caliper Life Science, Hopkinton, MA, USA). Spectral libraries were created acquiring spectra from 420 to 720 nm at 20 nm intervals from single staining with DAB, Vector Blue, Vector Red and hematoxylin. Spectral data sets from triple staining and control slides were acquired at the same wavelengths. To analyze the frequency of proliferating hepatocytes, MSI data sets were analyzed with InForm 1.4 image analysis software (PerkinElmer/Caliper Life Science) as earlier described for proliferating hepatocytes in rabbit liver by Van der Loos.[47] The learn-by-example interface from the software segments hepatocytic and sinusoidal tissue compartments. Next, the number of proliferating hepatocytes was calculated by analyzing the number of cells in the hepatocytic tissue compartment with coexpression for cytoplasmic CK18 (Vector Red) and nuclear Ki67 (Vector Blue). For comparison and validation of the automated procedure, two independent observers manually counted all Ki67-positive hepatocytes in the images that were used to create the algorithm.

RNA isolation, qRT-PCR, siRNA and miRNA Taqman assay

To determine ApoB mRNA knockdown, gene expression and siApoB expression *in vivo*, total RNA was isolated from frozen liver sections at 8 weeks p.i. using Trizol (Invitrogen, Carlsbad, CA, USA). Genomic DNA was removed by DNAse treatment using TURBO DNase (Ambion, Austin, TX, USA). First-strand complementary DNA was reverse transcribed using random hexamer primers with the Dynamo kit (Finnzymes, Espoo, Finland). Real-time PCR amplification was performed with gene-specific primers. PCR reaction conditions were: 95 °C for 10 min, followed by 40 cycles of 15 s at 95 °C and 1 min at 60 °C. The assays were performed on ABI 7000 or ABI 7500 (Applied Biosystems, Foster City, CA, USA). Gene expression levels were normalized to β-actin as an internal control, and the relative gene expression $2^{-\Delta\Delta Ct}$ method of Livak and Schmittgen[48] was used for analysis of PCR data. All sequences of primers used in this study are listed in Supplementary Table 6.

NGS and functional analysis of liver transcriptome

To analyze liver transcriptome, total RNA was isolated from frozen liver sections of representative animals at 8 weeks p.i. with AAV-shApoB, AAV-miApoB, AAV-shScr, AAV-miScr or PBS using Trizol (Invitrogen). Transcriptome NGS was carried out by Macrogen Inc. (Seoul, Korea) on an Illumina HiSeq 2000 platform (Illumina, San Diego, CA, USA). The amount of reads for each sample was: shScr (43926136), shApoB (46123849), miScr (39480829), miApoB (61959736) and PBS (36756817). The library preparation and the data analysis have been described before.

For the ApoB functional interactions, online database resource search tool for the retrieval of interacting genes (STRING) was used, which allowed annotation of functional interactions of ApoB protein in cell (http://string-db.org/).[49] For the genes that were identified, RPKM gene expression values were compared with shScr and miScr. As the next step, fold change between sample and control was calculated. Upregulation of genes (fold change >1.5) was marked in green and downregulations (fold change <-1.5) were marked in red.

For the transcriptome analysis, RPKM gene expression values were compared with PBS using Kal's test (*Z*-test) with Bonferroni correction. All genes that changed significantly ($P<0.05$) and were expressed as >0.1 (RPKM >0.1) were included in the further analysis. Functional analysis of the significantly changing genes was done with the functional annotation tool DAVID (v6.7; National Institute of Allergy and Infectious Diseases, NIH) that allows finding combination of coocurrent genes under study with respect to a reference list.[50,51] The annotations were done simultaneously with the reference to Gene Ontology databases (GOTERM_BP_FAT and GOTERM_MF_FAT, www.geneontology.org) and to KEGG pathway database (KEGG_PATHWAY; www.genome.ad.jp/kegg/pathway.html). The redundancy in the gene list was manually analyzed and significant annotations were grouped in eight categories and the percentage of genes in each category was calculated with reference to all genes that were annotated in DAVID analysis.

CONFLICT OF INTEREST

The authors declare no conflict of interest.

ACKNOWLEDGEMENTS

This work was carried out and funded by uniQure Biopharma B.V.

REFERENCES

1 Fire A, Xu S, Montgomery MK, Kostas SA, Driver SE, Mello CC. Potent and specific genetic interference by double-stranded RNA in Caenorhabditis elegans. *Nature* 1998; **391**: 806–811.
2 Paddison PJ, Caudy AA, Bernstein E, Hannon GJ, Conklin DS. Short hairpin RNAs (shRNAs) induce sequence-specific silencing in mammalian cells. *Genes Dev* 2002; **16**: 948–958.
3 Soutschek J, Akinc A, Bramlage B, Charisse K, Constien R, Donoghue M *et al.* Therapeutic silencing of an endogenous gene by systemic administration of modified siRNAs. *Nature* 2004; **432**: 173–178.
4 Boudreau RL, Martins I, Davidson BL. Artificial microRNAs as siRNA shuttles: improved safety as compared to shRNAs in vitro and in vivo. *Mol Ther* 2009; **17**: 169–175.
5 Zamore PD, Tuschl T, Sharp PA, Bartel DP. RNAi: double-stranded RNA directs the ATP-dependent cleavage of mRNA at 21–23 nucleotide intervals. *Cell* 2000; **101**: 25–33.
6 Bartel DP. MicroRNAs: genomics, biogenesis, mechanism, and function. *Cell* 2004; **116**: 281–297.
7 Borel F, van Logtenstein R, Koornneef A, Maczuga P, Ritsema T, Petry H *et al.* In vivo knock-down of multidrug resistance transporters ABCC1 and ABCC2 by AAV-delivered shRNAs and by artificial miRNAs. *J RNAi Gene Silencing* 2011; **7**: 434–442.
8 Grimm D, Streetz KL, Jopling CL, Storm TA, Pandey K, Davis CR *et al.* Fatality in mice due to oversaturation of cellular microRNA/short hairpin RNA pathways. *Nature* 2006; **441**: 537–541.
9 Ahn M, Witting SR, Ruiz R, Saxena R, Morral N. Constitutive expression of shRNA in vivo triggers build up of mature hairpin molecules. *Hum Gene Ther* 2011; **22**: 1483–1497.
10 Bridge AJ, Pebernard S, Ducraux A, Nicoulaz AL, Iggo R. Induction of an interferon response by RNAi vectors in mammalian cells. *Nat Genet* 2003; **34**: 263–264.
11 Sledz CA, Holko M, de Veer MJ, Silverman RH, Williams BR. Activation of the interferon system by short-interfering RNAs. *Nat Cell Biol* 2003; **5**: 834–839.
12 Jackson AL, Bartz SR, Schelter J, Kobayashi SV, Burchard J, Mao M *et al.* Expression profiling reveals off-target gene regulation by RNAi. *Nat Biotechnol* 2003; **21**: 635–637.
13 McBride JL, Boudreau RL, Harper SQ, Staber PD, Monteys AM, Martins I *et al.* Artificial miRNAs mitigate shRNA-mediated toxicity in the brain: Implications for the therapeutic development of RNAi. *Proc Natl Acad Sci USA* 2008; **105**: 5868–5873.
14 Giering JC, Grimm D, Storm TA, Kay MA. Expression of shRNA from a tissue-specific pol II promoter is an effective and safe RNAi therapeutic. *Mol Ther* 2008; **16**: 1630–1636.
15 Maczuga P, Koornneef A, Borel F, Petry H, van Deventer S, Ritsema T *et al.* Optimization and comparison of knockdown efficacy between polymerase II expressed shRNA and artificial miRNA targeting luciferase and Apolipoprotein B100. *BMC Biotechnol* 2012; **12**: 42.
16 Judge AD, Sood V, Shaw JR, Fang D, McClintock K, MacLachlan I. Sequence-dependent stimulation of the mammalian innate immune response by synthetic siRNA. *Nat Biotech* 2005; **23**: 457–462.
17 Kariko K, Bhuyan P, Capodici J, Ni H, Lubinski J, Friedman H *et al.* Exogenous siRNA mediates sequence-independent gene suppression by signaling through toll-like receptor 3. *Cells Tissues Organs* 2004; **177**: 132–138.
18 Kleinman ME, Yamada K, Takeda A, Chandrasekaran V, Nozaki M, Baffi JZ *et al.* Sequence- and target-independent angiogenesis suppression by siRNA via TLR3. *Nature* 2008; **452**: 591–597.
19 Witting SR, Brown M, Saxena R, Nabinger S, Morral N. Helper-dependent adenovirus-mediated short hairpin RNA expression in the liver activates the interferon response. *J Biol Chem* 2008; **283**: 2120–2128.
20 Kenworthy R, Lambert D, Yang F, Wang N, Chen Z, Zhu H *et al.* Short-hairpin RNAs delivered by lentiviral vector transduction trigger RIG-I-mediated IFN activation. *Nucleic Acids Res* 2009; **37**: 6587–6599.
21 Jackson AL, Linsley PS. Recognizing and avoiding siRNA off-target effects for target identification and therapeutic application. *Nat Rev Drug Discov* 2010; **9**: 57–67.
22 Boudreau RL, Spengler RM, Davidson BL. Rational design of therapeutic siRNAs: minimizing off-targeting potential to improve the safety of RNAi therapy for Huntington's disease. *Mol Ther* 2011; **19**: 2169–2177.

23 Caffrey DR, Zhao J, Song Z, Schaffer ME, Haney SA, Subramanian RR *et al.* siRNA off-target effects can be reduced at concentrations that match their individual potency. *PLoS One* 2011; **6**: e21503.
24 Maczuga P, Lubelski J, van Logtenstein R, Borel F, Blits B, Fakkert E *et al.* Embedding siRNA sequences targeting Apolipoprotein B100 in shRNA and miRNA scaffolds results in differential processing and in vivo efficacy. *Mol Ther* 2013; **21**: 217–227.
25 Young SG. Recent progress in understanding apolipoprotein B. *Circulation* 1990; **82**: 1574–1594.
26 Rozema DB, Lewis DL, Wakefield DH, Wong SC, Klein JJ, Roesch PL *et al.* Dynamic PolyConjugates for targeted in vivo delivery of siRNA to hepatocytes. *Proc Natl Acad Sci USA* 2007; **104**: 12982–12987.
27 Tarugi P, Averna M, Di LE, Cefalu AB, Noto D, Magnolo L *et al.* Molecular diagnosis of hypobetalipoproteinemia: an ENID review. *Atherosclerosis* 2007; **195**: e19–e27.
28 Visser ME, Akdim F, Tribble DL, Nederveen AJ, Kwoh TJ, Kastelein JJ *et al.* Effect of apolipoprotein-B synthesis inhibition on liver triglyceride content in patients with familial hypercholesterolemia. *J Lipid Res* 2010; **51**: 1057–1062.
29 Rawlings ND, Tolle DP, Barrett AJ. Evolutionary families of peptidase inhibitors. *Biochem J* 2004; **378**: 705–716.
30 Silverman GA, Bird PI, Carrell RW, Church FC, Coughlin PB, Gettins PG *et al.* The serpins are an expanding superfamily of structurally similar but functionally diverse proteins. Evolution, mechanism of inhibition, novel functions, and a revised nomenclature. *J Biol Chem* 2001; **276**: 33293–33296.
31 Irving JA, Pike RN, Lesk AM, Whisstock JC. Phylogeny of the serpin superfamily: implications of patterns of amino acid conservation for structure and function. *Genome Res* 2000; **10**: 1845–1864.
32 Martin LJ, Tremblay JJ. The nuclear receptors NUR77 and SF1 play additive roles with c-JUN through distinct elements on the mouse Star promoter. *J Mol Endocrinol* 2009; **42**: 119–129.
33 Shao Q, Shen LH, Hu LH, Pu J, Qi MY, Li WQ *et al.* Nuclear receptor Nur77 suppresses inflammatory response dependent on COX-2 in macrophages induced by oxLDL. *J Mol Cell Cardiol* 2010; **49**: 304–311.
34 Bermudez O, Pages G, Gimond C. The dual-specificity MAP kinase phosphatases: critical roles in development and cancer. *Am J Physiol Cell Physiol* 2010; **299**: C189–C202.
35 Suhy DA, Kao SC, Mao T, Whiteley L, Denise H, Souberbielle B *et al.* Safe, long-term hepatic expression of anti-HCV shRNA in a nonhuman primate model. *Mol Ther* 2012; **20**: 1737–1749.
36 Tadin-Strapps M, Peterson LB, Cumiskey AM, Rosa RL, Mendoza VH, Castro-Perez J *et al.* siRNA induced liver ApoB knockdown lowers serum LDL-cholesterol in a mouse model with human-like serum lipids. *J Lipid Res* 2011; **52**: 1084–1097.
37 Zimmermann TS, Lee AC, Akinc A, Bramlage B, Bumcrot D, Fedoruk MN *et al.* RNAi-mediated gene silencing in non-human primates. *Nature* 2006; **441**: 111–114.
38 Crooke RM, Graham MJ, Lemonidis KM, Whipple CP, Koo S, Perera RJ. An apolipoprotein B antisense oligonucleotide lowers LDL cholesterol in hyperlipidemic mice without causing hepatic steatosis. *J Lipid Res* 2005; **46**: 872–884.
39 Tep S, Mihaila R, Freeman A, Pickering V, Huyhn F, Tadin-Strapps M *et al.* Rescue of Mtp siRNA-induced hepatic steatosis by DGAT2 siRNA silencing. *J Lipid Res* 2012; **53**: 859–867.
40 Savary S, Trompier D, Andreoletti P, Le BF, Demarquoy J, Lizard G. Fatty acids-induced lipotoxicity and inflammation. *Curr Drug Metab* 2012; **13**: 1358–1370.
41 Penaud-Budloo M, Le Guiner C, Nowrouzi A, Toromanoff A, Cherel Y, Chenuaud P *et al.* Adeno-associated virus vector genomes persist as episomal chromatin in primate muscle. *J Virol* 2008; **82**: 7875–7885.
42 Flood C, Gustafsson M, Pitas RE, Arnaboldi L, Walzem RL, Boren J. Molecular mechanism for changes in proteoglycan binding on compositional changes of the core and the surface of low-density lipoprotein-containing human apolipoprotein B100. *Arterioscler Thromb Vasc Biol* 2004; **24**: 564–570.
43 Olivecrona G, Olivecrona T. Triglyceride lipases and atherosclerosis. *Curr Opin Lipidol* 2010; **21**: 409–415.
44 Okuyama S, Marusawa H, Matsumoto T, Ueda Y, Matsumoto Y, Endo Y *et al.* Excessive activity of apolipoprotein B mRNA editing enzyme catalytic polypeptide 2 (APOBEC2) contributes to liver and lung tumorigenesis. *Int J Cancer* 2012; **130**: 1294–1301.
45 Mikl MC, Watt IN, Lu M, Reik W, Davies SL, Neuberger MS *et al.* Mice deficient in APOBEC2 and APOBEC3. *Mol Cell Biol* 2005; **25**: 7270–7277.
46 Koornneef A, Maczuga P, van Logtenstein R, Borel F, Blits B, Ritsema T *et al.* Apolipoprotein B knockdown by AAV-delivered shRNA lowers plasma cholesterol in mice. *Mol Ther* 2011; **19**: 731–740.
47 van der Loos CM. Multiple immunoenzyme staining: methods and visualizations for the observation with spectral imaging. *J Histochem Cytochem* 2008; **56**: 313–328.
48 Livak KJ, Schmittgen TD. Analysis of relative gene expression data using real-time quantitative PCR and the 2-[delta][delta]CT method. *Methods* 2001; **25**: 402–408.
49 Szklarczyk D, Franceschini A, Kuhn M, Simonovic M, Roth A, Minguez P *et al.* The STRING database in 2011: functional interaction networks of proteins, globally integrated and scored. *Nucleic Acids Res* 2011; **39**: D561–D568.
50 Huang d W, Sherman BT, Lempicki RA. Systematic and integrative analysis of large gene lists using DAVID bioinformatics resources. *Nat Protoc* 2009; **4**: 44–57.
51 Huang d W, Sherman BT, Lempicki RA. Bioinformatics enrichment tools: paths toward the comprehensive functional analysis of large gene lists. *Nucleic Acids Res* 2009; **37**: 1–13.

Supplementary Information accompanies this paper on Gene Therapy website (http://www.nature.com/gt)